RAA 2017 Vol. **17** No. **6**, 61 (10pp) doi: 10.1088/1674–4527/17/6/61

http://www.raa-journal.org *http://iopscience.iop.org/raa*

***R**esearch in*
***A**stronomy and*
***A**strophysics*

General relativistic calculations for white dwarfs

Arun Mathew and Malay K. Nandy

Department of Physics, Indian Institute of Technology Guwahati, Guwahati 781 039, India; *a.mathew@iitg.ernet.in*, *mknandy@iitg.ernet.in*

Received 2016 October 26; accepted 2017 March 17

Abstract The mass-radius relations for white dwarfs are investigated by solving the Newtonian as well as Tolman-Oppenheimer-Volkoff (TOV) equations for hydrostatic equilibrium assuming the electron gas to be non-interacting. We find that the Newtonian limiting mass of $1.4562\,M_\odot$ is modified to $1.4166\,M_\odot$ in the general relativistic case for $^4_2$He (and $^{12}_6$C) white dwarfs. Using the same general relativistic treatment, the critical mass for $^{56}_{26}$Fe white dwarfs is obtained as $1.2230\,M_\odot$. In addition, departure from the ideal degenerate equation of state (EoS) is accounted for by considering Salpeter's EoS along with the TOV equation, yielding slightly lower values for the critical masses, namely $1.4081\,M_\odot$ for $^4_2$He, $1.3916\,M_\odot$ for $^{12}_6$C and $1.1565\,M_\odot$ for $^{56}_{26}$Fe white dwarfs. We also compare the critical densities for gravitational instability with the neutronization threshold densities to find that $^4_2$He and $^{12}_6$C white dwarfs are stable against neutronization with the critical values of $1.4081\,M_\odot$ and $1.3916\,M_\odot$, respectively. However, the critical masses for $^{16}_8$O, $^{20}_{10}$Ne, $^{24}_{12}$Mg, $^{28}_{14}$Si, $^{32}_{16}$S and $^{56}_{26}$Fe white dwarfs are lower due to neutronization. Corresponding to their central densities for neutronization thresholds, we obtain their maximum stable masses due to neutronization by solving the TOV equation coupled with the Salpeter EoS.

Key words: equation of state — hydrodynamics — instabilities — relativistic processes — stars: white dwarfs

1 INTRODUCTION

Following the formulation of Fermi-Dirac statistics, Fowler (1926) treated the electron gas in Sirius B as a degenerate non-relativistic gas and found no limiting mass for the star. However, Anderson (1929) and Stoner (1929) considered the electron gas as relativistic and found the existence of a limiting density, although their treatments were heuristic. Chandrasekhar (1931b,a, 1935, 1939) obtained the limiting mass of $0.91\,M_\odot$ initially by treating the degenerate electron gas as relativistic, and subsequently he succeeded in formulating the theory of white dwarfs to full generality. He employed Newtonian gravity and an equation of state (EoS) valid for the entire range of electron velocities (including relativistic velocities) of the degenerate Fermi gas to obtain the equation of hydrostatic equilibrium. He thus obtained equations in the form of the Lane-Emden equation with index 3 and solved the differential equations numerically to obtain the limiting mass of $1.44\,M_\odot$. Chandrasekhar & Tooper (1964) also considered the problem in the general relativistic framework to study the instability of a radially pulsating white dwarf to yield the critical mass of $1.4176\,M_\odot$. Anand (1965) studied the effect of rotation on a white dwarf and showed that the value of limiting mass increases to $1.704\,M_\odot$. Qualitative arguments given by Landau & Lifshitz (1980) suggest that the inter-particle Coulomb interaction is negligible in a white dwarf. Using the method of Bohm & Pines (1951), Singh (1957) demonstrated that the correction to the electron density due to electron-electron interaction is small and can be treated as negligible. On the other hand, Salpeter (1961) reconsidered the problem to account for Coulomb effects, Thomas-Fermi correction, exchange energy and correlation energy, and found that the EoS departs measurably from the ideal degenerate case.

In deriving the general relativistic equation of equilibrium for compact stars, Tolman (1939) and Oppenheimer & Volkoff (1939) showed how the Newtonian equation of hydrostatic equilibrium is modified into what is known as the Tolman-Oppenheimer-Volkoff (TOV) equation. They considered the energy-momentum tensor for a perfect fluid in the Einstein's field equation and solved for the metric for the interior of the star. This resulted in a set of three differential equations in four unknown functions, which are incomplete unless provided with the EoS. While Tolman obtained the interior solution for a few different analytically tractable cases, Oppenheimer and Volkoff numerically solved those equations for massive neutron cores by taking the full EoS and treating it as a non-interacting Fermi (neutron) gas.

In this paper, we consider the hydrostatic equilibrium of white dwarfs and obtain the mass-radius relationship by solving the TOV equation. It is found, for large values of central densities, that the Newtonian limit of $1.4562\,M_\odot$ is decreased to $1.4166\,M_\odot$ for $^4_2$He (and $^{12}_6$C) white dwarfs in the general relativistic treatment, assuming the electron gas to be ideally degenerate. Furthermore, the critical mass for $^{56}_{26}$Fe white dwarfs is found to be $1.2230\,M_\odot$ in the same formulation. We also consider the effect of Coulomb interaction and other types of interactions by considering the Salpeter EoS in the same general relativistic formulation to obtain the critical masses of $1.4081\,M_\odot$ for $^4_2$He, $1.3916\,M_\odot$ for $^{12}_6$C and $1.1565\,M_\odot$ for $^{56}_{26}$Fe white dwarfs.

We have also obtained the critical densities for gravitational instability directly from the solution of the TOV equation coupled with Salpeter EoS and compare them with the neutronization thresholds. We find that $^4_2$He and $^{12}_6$C white dwarfs are stable against neutronization with the critical values of $1.4081\,M_\odot$ and $1.3916\,M_\odot$ respectively, whereas for $^{16}_8$O, $^{20}_{10}$Ne, $^{24}_{12}$Mg, $^{28}_{14}$Si, $^{32}_{16}$S and $^{56}_{26}$Fe white dwarfs, the critical masses for stability are smaller due to neutronization. For these white dwarfs, we have also obtained the maximum stable masses due to neutronization by solving the TOV equation coupled with the Salpeter EoS corresponding to their central densities for neutronization thresholds.

The rest of the paper is organized as follows. In Section 2, we outline the derivation of the TOV equation for a perfect fluid in equilibrium in general relativity. The problem of white dwarfs is taken up by considering the EoS of cold degenerate electron gas. We also include the case of Salpeter EoS to account for the non-ideal nature of the electron gas. The non-linear coupled differential equations so obtained are solved numerically in Section 3, where the equations following from Newtonian gravity are also solved for the purpose of comparison. The mass-radius relationships obtained in the two cases are also compared. In Section 4, the instabilities due to gravitation and inverse beta decay are examined. The critical masses for neutronization thresholds are computed for a few relevant stars by solving the TOV equation coupled with Salpeter EoS. The numerical results are presented with a few relevant plots and tables.

2 GENERAL RELATIVISTIC HYDROSTATIC EQUILIBRIUM

The interior of a spherically symmetric star is described by

$$ds^2 = e^{\nu}dt^2 - e^{\lambda}dr^2 - r^2d\theta^2 - r^2\sin^2\theta\,d\phi^2,$$

where ν and λ are functions of the radial distance r for the static case. The matter inside the star is considered to be a perfect fluid with energy-momentum tensor

$$T_{\alpha\beta} = (\varepsilon + p)u_\alpha u_\beta - pg_{\alpha\beta},$$

where p is the pressure and $\varepsilon = \rho c^2$ is the mass-energy density. Tolman (1939) and Oppenheimer & Volkoff (1939) considered the corresponding Einstein's field equations in the interior part of the star and solved them with the boundary condition of the Schwarzschild solution in the exterior region. They obtained

$$e^{\nu(r)} = \left(1 - \frac{G}{c^2}\frac{2M}{R}\right)\exp\left[-2\int_0^{p(r)}\frac{dp}{p+\varepsilon(p)}\right],$$

$$e^{-\lambda} = 1 - \frac{G}{c^2}\frac{2m(r)}{r}$$

and

$$\frac{dp}{dr} = -\frac{\varepsilon(r)+p(r)}{2}\frac{d\nu}{dr}.$$

These solutions lead to the well-known TOV equation, namely

$$\frac{dp(r)}{dr} = -\frac{G}{c^2}\frac{\varepsilon(r)+p(r)}{r(r-\frac{2G}{c^2}m(r))}\left[m(r) + \frac{4\pi}{c^2}p(r)r^3\right] \tag{1}$$

with

$$\frac{dm(r)}{dr} = \frac{4\pi}{c^2}\varepsilon(r)r^2. \tag{2}$$

Equations (1) and (2), together with the EoS of matter $\varepsilon = \varepsilon(p)$, determine the hydrostatic equilibrium for an isotropic general relativistic non-rotating fluid sphere.

In a white dwarf, the electrons can be treated as an ideal degenerate Fermi gas to a good approximation. The corresponding EoS is given by the parametric forms

$$\begin{aligned}
\varepsilon(\xi) &= \tfrac{32\mu_e H}{3m_e} K \sinh^3\tfrac{\xi}{4} f(\xi),\\
p(\xi) &= \tfrac{1}{3}K\left(\sinh\xi - 8\sinh\tfrac{\xi}{2} + 3\xi\right), \qquad (3)\\
f(\xi) &= 1 + \tfrac{3m_e(\sinh\xi-\xi)}{32\mu_e H\sinh^3\frac{\xi}{4}} - \tfrac{m_e}{\mu_e H},
\end{aligned}$$

where $\xi = 4\sinh^{-1}(\frac{p_F}{m_e c})$, $K = \frac{\pi m_e^4 c^5}{4h^3}$, $\mu_e = A/Z$ is the number of nucleons per electron and H is the atomic mass unit. These equations are valid for all values of electron velocities, including extreme relativistic velocities. Substituting the set of Equations (3) in Equations (1) and (2), the following differential equations are obtained.

$$\begin{aligned}
\frac{dm}{dr} &= 4\pi\frac{32\mu_e H}{3m_e}\frac{K}{c^2}r^2\sinh^3\frac{\xi}{4}f(\xi),\\
\frac{d\xi}{dr} &= -\frac{32\,G\mu_e H}{m_e c^2(\cosh\xi - 4\cosh\frac{\xi}{2}+3)r}\\
&\quad\Big[\sinh^3\frac{\xi}{4}f(\xi) + \frac{m_e}{32\mu_e H}\\
&\quad(\sinh\xi - 8\sinh\frac{\xi}{2} + 3\xi)\Big]\times\Big[m(r)\\
&\quad + \frac{4\pi K(\sinh\xi - 8\sinh\frac{\xi}{2}+3\xi)r^3}{3c^2}\Big]\\
&\quad\Big[r - \frac{2Gm(r)}{c^2}\Big]^{-1}. \qquad (4)
\end{aligned}$$

The two differential equations in (4) are valid when the electron gas is treated as an ideal degenerate Fermi gas. A more realistic treatment must include interactions among the electrons and nuclei. Salpeter (1961) considered this situation and included the Coulomb effects, Thomas-Fermi correction, exchange energy and correlation energy to arrive at an EoS, given by

$$\begin{aligned}
\varepsilon_{\rm Coul} &= -\frac{9}{10}\left(\frac{4}{9\pi}\right)^{1/3}\alpha\, Z^{2/3}\sinh^4\frac{\xi}{4},\\
\varepsilon_{\rm TF} &= -\frac{162}{175}\left(\frac{4}{9\pi}\right)^{2/3}\alpha^2\, Z^{4/3}\sinh^3\frac{\xi}{4}\cosh\frac{\xi}{4},\\
\varepsilon_{\rm ex} &= -\frac{3}{128\pi}\,\alpha\left(12\xi\sinh\frac{\xi}{2} - 16\cosh\frac{\xi}{2}\right.\\
&\quad\left. -2e^{\frac{\xi}{4}}\cosh^3\frac{\xi}{4} - 3\xi^2 + 18\right),\\
\varepsilon_{\rm corr} &= \alpha^2\,\sinh^3\frac{\xi}{4}\\
&\quad\left(0.0115 + 0.031\log_e\left[\alpha\,\sinh^{-1}\frac{\xi}{4}\right]\right) \qquad (5)
\end{aligned}$$

in the units of $\frac{32}{3}K$, and

$$\begin{aligned}
p_{\rm Coul} &= -\frac{16}{5}\left(\frac{4}{9\pi}\right)^{1/3}\alpha\, Z^{2/3}\sinh^4\frac{\xi}{4},\\
p_{\rm TF} &= -\frac{576}{175}\left(\frac{4}{9\pi}\right)^{2/3}\alpha^2\, Z^{4/3}\sinh^5\frac{\xi}{4}\,\mathrm{sech}\,\frac{\xi}{4},\\
p_{\rm ex} &= \frac{\alpha}{2\pi}\Big[\cosh\xi + 8\cosh\frac{\xi}{2} - 6\xi\sinh\frac{\xi}{2}\\
&\quad + \frac{3}{2}\xi^2 - 9 - \frac{4}{3}\tanh\frac{\xi}{4}\Big(\sinh\xi\\
&\quad -2\sinh\frac{\xi}{2} - 3\xi\cosh\frac{\xi}{2} + 3\xi\Big)\Big],\\
p_{\rm corr} &= -\frac{32}{9}0.0311\,\alpha^2\,\sinh^3\frac{\xi}{4} \qquad (6)
\end{aligned}$$

in the units of K, where Z is the number of protons and A is the total number of nucleons in a nucleus.

3 NUMERICAL SOLUTIONS

We shall solve the TOV equations for two cases, namely, the ideal degenerate case and the non-ideal case, in this section.

3.1 Ideal Degenerate Case

When the electron gas is assumed to form an ideal degenerate Fermi gas, the TOV equations given by the set of Equations in (1) and (2) are coupled with the EoS given by the set of Equations in (3). The resulting equations in (4) can be made dimensionless by introducing dimensionless variables $x = r/R_{\rm scale}$ and $u = m/M_{\rm scale}$. They reduce to the forms

$$\frac{du}{dx} = x^2\sinh^3\left(\frac{\xi}{4}\right)f(\xi), \qquad (7)$$

$$\begin{aligned}
\frac{d\xi}{dx} &= -\frac{1}{(\cosh\xi - 4\cosh\frac{\xi}{2}+3)x}\Big[\sinh^3\frac{\xi}{4}f(\xi)\\
&\quad + \frac{m_e}{32\mu_e H}\Big(\sinh\xi - 8\sinh\frac{\xi}{2} + 3\xi\Big)\Big]\\
&\quad\Big[u(x) + \frac{m_e}{32\mu_e H}\Big(\sinh\xi - 8\sinh\frac{\xi}{2} + 3\xi\Big)x^3\Big]\\
&\quad\Big[x - \frac{m_e}{16\mu_e H}\,u(x)\Big]^{-1}. \qquad (8)
\end{aligned}$$

We have chosen the values $R_{\rm scale} = 2.3788\mu_e^{-1}\times 10^8$ cm and $M_{\rm scale} = 1.6475\,\mu_e^{-2}\times 10^{32}$ g so that the prefactors in Equations (7) and (8) are normalized to unity. As an analytical solution is not possible, we employ the fourth-order Runge-Kutta scheme [Press (1988)] to integrate them simultaneously. Solutions to these equations

Table 1 Mass, Radius, Central Density ρ_0 and Central Pressure p_0 for Various Values of ξ_0 for $^4_2$He White Dwarfs

ξ_0	$\left(\frac{p_F}{m_e c}\right)_0$	Mass ($M_\odot$)	Radius (km)	ρ_0 (2×10^{10} g cm^{-3})	p_0 (2×10^{28} dyn cm^{-2})
(1)	(2)	(3)	(4)	(5)	(6)
2.35	0.6219	0.2957	12538.45	2.3425×10^{-5}	3.9601×10^{-7}
6.20	2.2496	0.9576	6015.35	1.1091×10^{-3}	1.3233×10^{-4}
15.28	22.7911	1.4166	1029.87	1.1581	1.6164
19.00	57.7878	1.3890	436.95	19.0131	66.9168
∞	∞	0.4583	52.23	∞	∞

are computed for several initial values of ξ_0 at the center of the star. Integration is carried out from the value $u = 0$, $\xi = \xi_0$ at $x = 0$ (center) to $x = x_b$ (surface) where $\xi_b = 0$ (which makes $p = 0$), and $u = u_b$. The first four entries in Table 1 display the results obtained in the range $1.0 \leq \xi_0 \leq 19.0$.

In the limit $\xi \to \infty$, Equations (7) and (8) reduce to the simple forms

$$\frac{du}{dx} = \frac{3m_e}{64\mu_e H} x^2 e^{\xi}, \tag{9}$$

$$\frac{d\xi}{dx} = -\frac{m_e}{8\mu_e H} \frac{1}{x(x - \frac{m_e}{32\mu_e H}\, 2u)} \left(u + \frac{m_e}{64\mu_e H} x^3 e^{\xi} \right). \tag{10}$$

From Equations (3), the ratio of central pressure to central mass-energy density for the limiting case $\xi \to \infty$ turns out to be $\frac{p}{\varepsilon} = \frac{1}{3}$, which represents a sphere of fluid with infinite density and pressure at the center. Equations (9) and (10) can be solved exactly to yield $u = \frac{48}{7} \left(\frac{\mu_e H}{m_e} \right) x$ and $e^{\xi} = \frac{1024}{7} \left(\frac{\mu_e H}{m_e} \right)^2 \frac{1}{x^2}$. From this solution, we get the initial condition (the ξ_0 value) to integrate Equations (7) and (8) from $\xi = \xi_0$ (center) to $\xi = 0$ (surface). An analysis of Equations (7) and (8) shows that they are well approximated by Equations (9) and (10) for $\xi \geq 55$ for $^4_2$He white dwarfs. The EoS $\frac{p}{\varepsilon} = \frac{1}{3}$ is also approached closely for $\xi \geq 55$. The last row in Table 1 corresponds to $\xi_0 = 55$.

To compare these results of numerical integration with results following from Newtonian gravity, we also numerically integrate the following (Newtonian) equations.

$$\frac{du}{dx} = x^2 \sinh^3 \frac{\xi}{4}, \tag{11}$$

$$\frac{d\xi}{dx} = -\frac{u(x) \sinh^3 \frac{\xi}{4}}{(\cosh \xi - 4 \cosh \frac{\xi}{2} + 3) x^2}. \tag{12}$$

The mass-radius relationships for $^4_2$He white dwarfs following from the numerical integrations of the TOV equations [(7) and (8)] and the Newtonian equations [(11) and (12)] are compared in Figure 1. It is seen that the two mass-radius curves coincide for small values of ξ_0. This is due to the fact that the TOV equation reduces to the Newtonian equation for small values of central densities as a result of negligible contribution from the internal energy and smallness of the metric correction $(2GM/c^2R)$. For small values of ξ_0, the EoS reduces to the form $p = C\rho^{5/3}$ and the mass-radius relation behaves as $M \sim R^{-3}$ in the right-hand part of the plot.

For higher values of central densities, the TOV curve starts to deviate from the Newtonian curve, as seen towards the left-hand part of the plot. Thus, for large ξ_0, there is a departure from the non-relativistic $M \sim R^{-3}$ behavior for both Newtonian and TOV cases. We also find that the critical mass is lower for the TOV case than the Newtonian case, with values being $1.4166\, M_\odot$ and $1.4562\, M_\odot$ respectively.

3.2 Non-ideal Case

A realistic treatment of the electron gas must include various types of interactions among the particles. We therefore consider the Salpeter EoS given by Equations (5) and (6) and couple them with the TOV equations [(1) and (2)]. A comparison between the ideal and non-ideal cases for the mass-radius relations of $^4_2$He white dwarfs is shown in Figure 2. As seen from the plot, the two curves do not coincide for any value of ξ_0, although the deviation becomes smaller for higher values of ξ_0. As a result, the critical value decreases to $1.4081\, M_\odot$, which is about 0.6% lower than the ideal value of $1.4166\, M_\odot$. We also observe that a $^{12}_6$C white dwarf acquires a critical mass of $1.3916\, M_\odot$, which is different from that of $^4_2$He ($1.4081\, M_\odot$) when the Salpeter EoS is taken into account.

Table 2 displays a comparison of the critical values of masses and radii for $^4_2$He, $^{12}_6$C and $^{56}_{26}$Fe white dwarfs.

We also solve the TOV equations [(1) and (2)] coupled with the Salpeter EoS [(5) and (6)] for $^{16}_8$O, $^{20}_{10}$Ne,

Table 2 Comparison of the critical values of masses and radii for $^4_2$He, $^{12}_6$C and $^{56}_{26}$Fe white dwarfs obtained by solving the TOV equations [(1) and (2)] coupled with the ideal EoS (3) and the Salpeter EoS [(5) and (6)].

	Critical mass ($M_\odot$)			Critical radius (km)		
	Ideal EoS	Salpeter EoS	% decrease	Ideal EoS	Salpeter EoS	% decrease
(1)	(2)	(3)	(4)	(5)	(6)	(7)
$^4_2$He	1.4166	1.4081	0.60	1029.87	1012.07	1.73
$^{12}_6$C	1.4166	1.3916	1.76	1029.87	1004.59	2.45
$^{56}_{26}$Fe	1.2230	1.1565	5.44	927.13	886.55	4.38

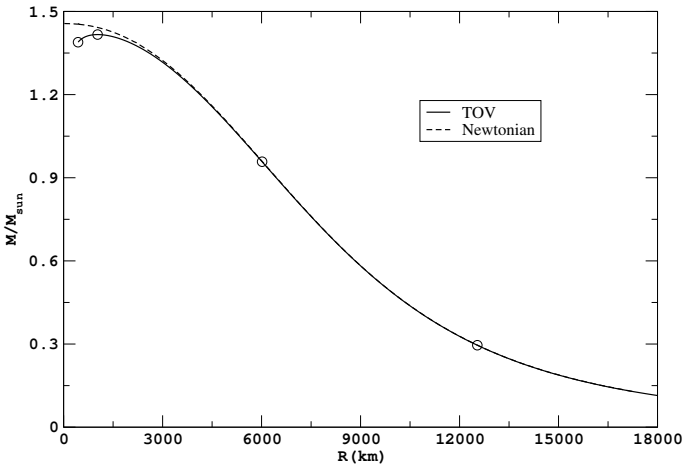

Fig. 1 Mass-Radius relationships given by the TOV (*solid curve*) and Newtonian (*dashed curve*) cases for $^4_2$He white dwarfs with ideal degenerate EoS. The data points shown encircled correspond to the first four entries in Table 1.

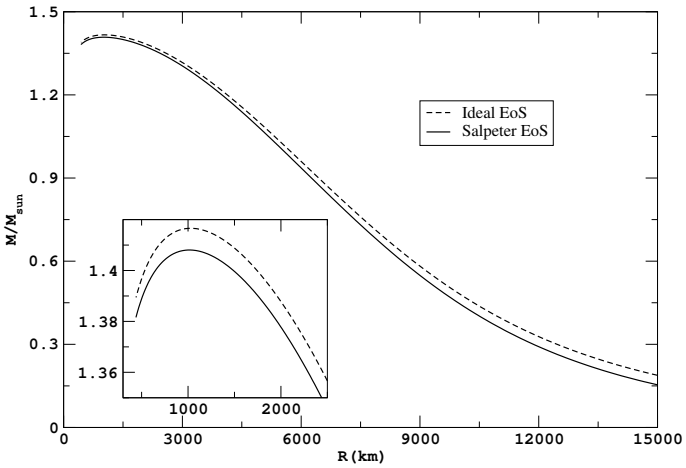

Fig. 2 Mass-Radius relationships given by the TOV equations for $^4_2$He white dwarfs. The dashed curve represents the solutions with ideal degenerate EoS and the solid curve represents the solutions with Salpeter EoS. The inset shows a magnified view around the region of the maxima in the two cases.

$^{24}_{12}$Mg, $^{28}_{14}$Si and $^{32}_{16}$S white dwarfs. The corresponding results are displayed in the fifth column of Table 3.

4 STABILITY OF WHITE DWARFS

In this section we shall consider gravitational instability as well as inverse β-decay instability for white dwarfs.

4.1 Gravitational Instability

The equilibrium configuration of the star is identified by the extremum in the energy-matter distribution curve. The total energy of the star was previously derived by Shapiro & Teukolsky (1983) by adding correction due

Table 3 Critical values in general relativity and neutronization thresholds for different white dwarfs. Here $\rho_c^{\rm ST}$ is the previous estimate [Shapiro & Teukolsky (1983)] of the critical central density, $\rho_c^{\rm TOVS}$ is the critical central density obtained from the TOV equations coupled with Salpeter EoS and ρ_β is the neutronization threshold density. The gravitational critical mass $M_c^{\rm TOVS}$ and the neutronization threshold mass $M_\beta^{\rm TOVS}$ follow from the solutions of the TOV equations coupled with Salpeter EoS for the corresponding central densities $\rho_c^{\rm TOVS}$ and ρ_β, respectively.

	$\rho_c^{\rm ST}$	$\rho_c^{\rm TOVS}$	ε_Z	ρ_β	$M_c^{\rm TOVS}$	$M_\beta^{\rm TOVS}$	% decrease
	$(2\times10^{10}\,{\rm g\,cm^{-3}})$	$(2\times10^{10}\,{\rm g\,cm^{-3}})$	(MeV)	$(2\times10^{10}\,{\rm g\,cm^{-3}})$	$(M_\odot)$	$(M_\odot)$	
(1)	(2)	(3)	(4)	(5)	(6)	(7)	(8)
$^4_2$He	1.3250	1.21150	20.596	6.85751	1.4081	—	—
$^{12}_6$C	1.3250	1.22060	13.370	1.94826	1.3916	—	—
$^{16}_8$O	1.3250	1.22979	10.419	0.94996	1.3849	1.3846	0.02
$^{20}_{10}$Ne	1.3250	1.26732	7.026	0.31036	1.3788	1.3702	0.62
$^{24}_{12}$Mg	1.3250	1.26730	5.513	0.15784	1.3731	1.3523	1.51
$^{28}_{14}$Si	1.3250	1.26728	4.643	0.09861	1.3677	1.3341	2.46
$^{32}_{16}$S	1.3250	1.26727	1.710	0.00370	1.3625	1.1649	14.50
$^{56}_{26}$Fe	1.5289	1.48186	3.695	0.05720	1.1565	1.0667	7.76

to general relativity, given by $E_T = E_{\rm int} + \Delta E_{\rm int} + E_{\rm Newt} + \Delta E_{\rm GR}$, where the first two terms correspond to the internal energy and the corresponding relativistic correction, the third term is the gravitational energy in the Newtonian limit, and the fourth term is the correction due to general relativity. The hydrostatic equations (11) and (12), based on Newtonian gravity, ignore the internal kinetic energy contribution and metric correction. Consequently, the general relativistic effects are taken into account by adding first order corrections in the above equation as shown. Thus, this expression for E_T is an approximate expression for energy due to the general relativistic correction. This approximation is expected to be good when the mass-radius ratio in the metric correction is small.

Minimizing this energy E_T yields the equilibrium condition $\frac{dE_T}{d\rho_0}|_{\rho_0=\rho_c} = 0$. Minima and maxima correspond to stable and unstable equilibria, given by $\frac{\partial M}{\partial \rho_0} > 0$ and $\frac{\partial M}{\partial \rho_0} < 0$, respectively. For $\frac{\partial M}{\partial \rho_0} < 0$, the electron degenerate pressure is smaller than the inward gravitational pull, causing the star to collapse continuously. The onset of this collapse was obtained by Shapiro & Teukolsky (1983) by setting $\frac{\partial^2 E_T}{\partial \rho_0^2} = 0$. Thus, the expression for the onset density of gravitational instability was calculated as

$$\rho_c^{\rm ST} = 2.646\times10^{10}\left(\frac{\mu_e}{2}\right)^2 {\rm g\,cm^{-3}}. \qquad (13)$$

At this critical value of the central density, the star becomes unstable against gravitational pull. As noted above, this expression for the onset density of gravitational instability is based on the above approximate expression for E_T. The critical values for the central density $\rho_c^{\rm ST}$ for a few white dwarfs following from Equation (13) are shown in Column (2) of Table 3.

In our present calculations, we take an alternative route to obtain the critical values for the central density, denoted by $\rho_c^{\rm TOVS}$. Thus, we obtain the critical central density $\rho_c^{\rm TOVS}$ from the solution of the full TOV equations [namely, Eqs. (1) and (2) coupled with the Salpeter EoS given by Eqs. (5) and (6)] without making any approximations. Hence, our results are expected to be close to exact.

The plot in Figure 3 shows the dependence of masses on the central densities ρ_0 of $^4_2$He and $^{56}_{26}$Fe white dwarfs as a result of computation based on the TOV equation coupled with Salpeter EoS. We see that the mass of the star increases with increase in the central density until a maximum is reached, beyond which it declines. The positive slope ($\frac{\partial M}{\partial \rho_0} > 0$) corresponds to the stable portion whereas the negative slope ($\frac{\partial M}{\partial \rho_0} < 0$) to the unstable portion. The plot also predicts the maximum stable masses a white dwarf can achieve, which are very nearly $1.4081\,M_\odot$ for $^4_2$He and $1.1565\,M_\odot$ for $^{56}_{26}$Fe white dwarfs. These correspond to central densities of $2.4230\times10^{10}\,{\rm g\,cm^{-3}}$ for $^4_2$He and $2.9637\times10^{10}\,{\rm g\,cm^{-3}}$ for $^{56}_{26}$Fe white dwarfs. For higher values of the densities, the stars become unstable and collapse under their own gravitational pull.

The occurrence of a critical mass can be clearly seen when we plot the mass M versus radius R of the star on linear scales. This is shown in Figure 4 for $^4_2$He, $^{12}_6$C and $^{56}_{26}$Fe white dwarfs, where the maxima are identified as the critical points, at masses of about $1.4081\,M_\odot$ for

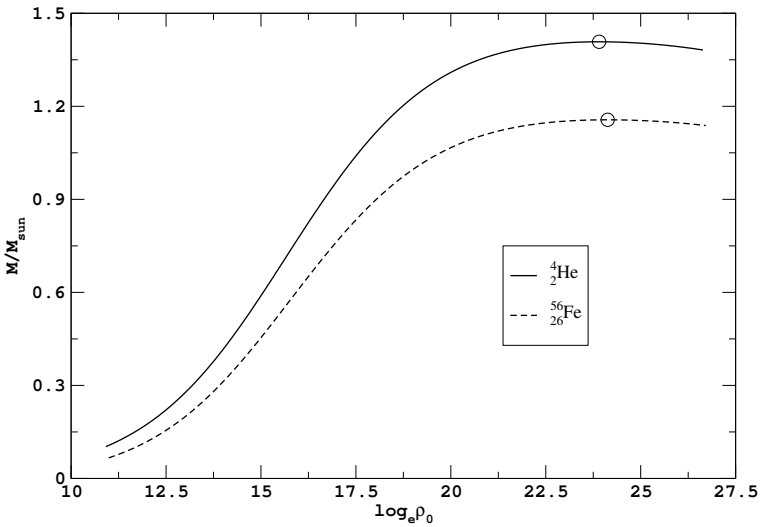

Fig. 3 Plots of M vs $\log_e \rho_0$ for $^4_2$He (*solid curve*) and $^{56}_{26}$Fe (*dashed curve*) white dwarfs obtained by solving the TOV equations [(1) and (2)] coupled with Salpeter EoS [(5) and (6)].

$^4_2$He, $1.3916\,M_\odot$ for $^{12}_6$C and for $1.1565\,M_\odot$ $^{56}_{26}$Fe white dwarfs. The portions towards the right of the maxima correspond to stable equilibria, whereas those towards the left correspond to instability.

The critical central densities $\rho_c^{\rm TOVS}$ for a few other white dwarfs ($^{16}_8$O, $^{20}_{10}$Ne, $^{24}_{12}$Mg, $^{28}_{14}$Si and $^{32}_{16}$S) are also computed numerically based on the TOV equation [(1) and (2)] coupled with the Salpeter EoS [(5) and (6)], and the results are shown in Column (3) of Table 3. In comparison to $\rho_c^{\rm ST}$, we see that the values for $\rho_c^{\rm TOVS}$ are lower in magnitude. The corresponding critical values for the masses $M_c^{\rm TOVS}$ following from the TOV equation coupled with the Salpeter EoS are displayed in Column (6) of Table 3.

4.2 Inverse β-Decay Instability

The process of inverse β-decay, namely

$$^A_Z X + e \longrightarrow {}^A_{Z-1}Y + \nu_e,$$

becomes important for high values of electron densities. This fact was ignored when calculating the most stable configurations admitted by gravity alone. At high electron densities, the electrons become more relativistic so that the condition $E_F \geqslant \varepsilon_Z$, where E_F is the Fermi energy and ε_Z is the difference in binding energies of the parent and daughter nuclei, may be satisfied for inverse β-decay to occur.

At a sufficiently high density, the star becomes unstable under inverse β-decay and collapses to form extremely dense matter (this might be a mixture of neutron rich nuclei, electrons and neutrons). The threshold density ρ_β for inverse β-decay was calculated by Salpeter (1961) by setting $E_F = \varepsilon_Z$. Rotondo et al. (2011) expressed it as

$$\rho_\beta = \frac{8\pi\mu_e H}{3h^3c^3}(\varepsilon_Z^2 + 2m_e c^2 \varepsilon_Z)^{3/2}. \qquad (14)$$

The β-decay energy ε_Z was obtained by least square fit to experimental data by Wapstra and Bos (1977) which was also used by Shapiro and Teukolsky (1983), as displayed in Column (4) of Table 3. The corresponding values of the threshold densities ρ_β following from Equation (14) are shown in Column (5) of Table 3.

For white dwarfs whose neutronization density ρ_β is smaller than the onset density of gravitational instability $\rho_c^{\rm TOVS}$, we expect an unstable phase before reaching the critical mass $M_c^{\rm TOVS}$ obtained from general relativity. Inverse β-decay that sets in before gravitational instability reduces the electron density, which in turn reduces the degeneracy pressure so that we expect a smaller value for the critical mass than that obtained by general relativity. Table 3 compares the critical central densities $\rho_c^{\rm TOVS}$ and inverse β-decay threshold densities ρ_β for white dwarfs with different compositions.

Comparing the threshold densities given in the third and fifth columns of Table 3, we see, for $^4_2$He and $^{12}_6$C white dwarfs, that gravitational instability sets in before neutronization instability can set in. This implies that the critical masses for $^4_2$He and $^{12}_6$C white dwarfs are $1.4081\,M_\odot$ and $1.3916\,M_\odot$, respectively. For all the other cases, threshold density ρ_β for neutronization starts

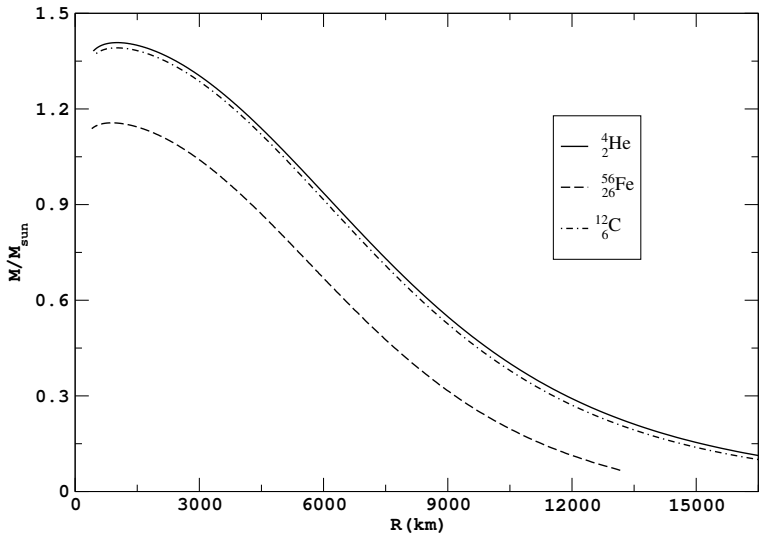

Fig. 4 Mass-radius relations for $^{4}_{2}$He (*solid curve*), $^{12}_{6}$C (*dot-dashed curve*) and $^{56}_{26}$Fe (*dashed curve*) white dwarfs obtained by solving TOV equations [(1) and (2)] coupled with Salpeter EoS [(5) and (6)].

before the critical density $\rho_c^{\rm TOVS}$ for gravitational instability is reached. This implies that the critical masses of $^{16}_{8}$O, $^{20}_{10}$Ne, $^{24}_{12}$Mg, $^{28}_{14}$Si, $^{32}_{16}$S and $^{56}_{26}$Fe white dwarfs must be lower than their corresponding critical mass for gravitational instability. We compute the corresponding masses for neutronization thresholds numerically from the TOV equations [(1) and (2)] coupled with Salpeter EoS [(5) and (6)], and identify them as the critical masses $M_\beta^{\rm TOVS}$ for stability against neutronization, which are shown in the seventh column of Table 3.

5 CONCLUSIONS

It is seen from our above investigations that general relativistic effects have lowered the limiting mass of a $^{4}_{2}$He white dwarf. In the ideal degenerate gas approximation, the new value ($1.4166\,M_\odot$) obtained by solving the TOV equation is not too far from the Newtonian limit ($1.4562\,M_\odot$). Thus the general relativistic effects are small in the case of a white dwarf, which lowers the limiting value by approximately 2.7%. Our calculated value of $1.4166\,M_\odot$ is slightly different from the results obtained by Bera & Bhattacharya (2016). They obtained $1.4158\,M_\odot$ and $1.4155\,M_\odot$ in two different general relativistic computations, which are approximately 2.36% and 2.38% lower than their Newtonian computation value of $1.45\,M_\odot$.

We note that the EoS is valid for all electron velocities, both non-relativistic and ultra-relativistic, connecting the two regimes smoothly. Although initially the inter-particle interaction was neglected by assuming an EoS for an ideal degenerate electron gas, we later incorporated it via the Salpeter EoS that includes Coulomb effects, Thomas-Fermi correction, exchange energy and correlation energy. When the TOV equations are solved incorporating these corrections, the critical mass turned out to be 1.4081 for $^{4}_{2}$He and 1.3916 for $^{12}_{6}$C white dwarfs, which are slightly lower than the ideal value ($1.4166\,M_\odot$). We have shown these differences in Table 3, which also include the values for the $^{56}_{26}$Fe white dwarf. The maxima of the mass-radius curve (in Fig. 4 and Fig. 2) mark the onset of gravitational collapse and the regions towards the left of the maxima correspond to unstable regions. It is expected that the growth in density makes the electrons more relativistic so that the condition favoring inverse beta decay is approached.

We took account of neutronization by using Equation (14) obtained on the basis of Salpeter's arguments. Values for the onset density ρ_β so obtained for inverse β-decay for different compositions of the star are shown in Column (5) of Table 3. A comparison with $\rho_c^{\rm TOVS}$ (shown in Column (3) of Table 3) indicates that stars composed of lighter elements ($^{4}_{2}$He and $^{12}_{6}$C) are more stable than those composed of heavier elements ($^{16}_{8}$O, $^{20}_{10}$Ne, $^{24}_{12}$Mg, $^{28}_{14}$Si, $^{32}_{16}$S and $^{56}_{26}$Fe). The onset of inverse β decay is found to start before reaching the onset of gravitational instability in white dwarfs composed of heavier elements. The maximum stable mass $M_c^{\rm TOVS}$ obtained by solving the TOV equations coupled with Salpeter EoS for these stars (as given in Column 6

of Table 3) no longer can be identified as their critical masses. Consequently for these stars, we solve the TOV equations coupled with Salpeter EoS corresponding to the central densities ρ_β to obtain the maximum stable mass $M_\beta^{\rm TOVS}$ as shown in the seventh column of Table 3.

Mass distribution of a large number of white dwarfs with a wide range of masses, including low mass and massive stars, was plotted by Bergeron et al. (2007) and Kepler et al. (2007). The most massive non-magnetic white dwarf observed was LHS4033 [Dahn et al. (2004); Bergeron et al. (2007); Kepler et al. (2007)] which was predicted to have an oxygen-neon core with a mass in the range of $1.318 - 1.335\,M_\odot$. This range of mass values is compatible with our calculations, as we see from the seventh column of Table 3.

However, recent observations of type Ia supernovae (SNe Ia) admit white dwarfs with masses as high as $2.3 - 2.6\,M_\odot$. Howell et al. (2006) argued that the over-luminosity and low expansion velocities around the SN 2003fg white dwarf could be explained if it is assumed to have a mass greater than $1.44\,M_\odot$. Hicken et al. (2007) presented SN2006gz as a possible SN Ia candidate that was identified with similar properties. Scalzo et al. (2010) estimated the total mass of the SN 2007if progenitor to be in the range $2.2 - 2.6\,M_\odot$. Silverman et al. (2011) suggested another member of the SNe Ia class, SN2009dc, with similar peculiarities, possibly formed from the merger of two white dwarfs.

It has been speculated that the presence of a magnetic field drastically modifies the situation in a compact star due to the Landau quantization of electronic energy levels. Gao et al. (2011) simulated electron β-capture in a magnetar by considering electrons belonging to the higher Landau levels in a super high magnetic field that admit the energy threshold values for inverse β-decay to occur. For a $^4_2$He white dwarf, Das & Mukhopadhyay (2012) considered the modified EoS due to the Landau levels of electrons in a magnetic field. They showed that a maximum mass of $2.3\ M_\odot$ is reached at the highest turning point in the mass-radius relation of a $^4_2$He white dwarf within the Newtonian (Lane-Emden) framework. They indicated that the presence of high magnetic fields can give rise to white dwarfs with masses as high as $2.3 - 2.6\ M_\odot$ and radii around 600 km. It is interesting to mention that Gao et al. (2013) and Zhu et al. (2016) provided a great deal of deliberations in this direction, particularly in the study of how the Fermi energy and the electron degeneracy pressure change in a neutron star due to the presence of a strong magnetic field.

Gao et al. (2013) and Li et al. (2016) indicated that, in the presence of a strong magnetic field, electron degeneracy pressure increases with strength of the magnetic field. This is because the pressure is proportional to E_F^4 and the Fermi energy E_F increases with the strength of the magnetic field. Consequently, the number density n_e (and hence the matter density), being determined by the Fermi energy, also increases with the magnetic field. Thus, with respect to the non-magnetic case, a greater matter density near and away from the center could be supported against gravitational pull by the increased pressure gradient in the presence of a strong magnetic field.

It may also be remarked that soft gamma ray repeaters (SGRs) and anomalous X-ray pulsars (AXPs) were thought to be magnetars until a recent exception was observed in SGR 0418+5729 which was found to be inconsistent with the magnetar model of SGRs and AXPs based on neutron stars. Malheiro et al. (2012) showed that the observed upper limit on the spin down rate of SGR 0418+5726 is in accordance with a model based on a massive fast rotating highly magnetized white dwarf. It may thus be speculated that their masses would be higher than $1.4562\ M_\odot$ due to the effect of strong magnetic field.

Acknowledgements M.K.N. is indebted to the Indian Institute of Technology Delhi for their kind hospitality during his visits.

References

Anand, S. P. S. 1965, Proceedings of the National Academy of Sciences, 54, 23
Anderson, W. 1929, Zeitschrift fur Physik, 56, 851
Bera, P., & Bhattacharya, D. 2016, MNRAS, 456, 3375
Bergeron, P., Gianninas, A., & Boudreault, S. 2007, in Astronomical Society of the Pacific Conference Series, 372, 15th European Workshop on White Dwarfs, ed. R. Napiwotzki & M. R. Burleigh, 29
Bohm, D., & Pines, D. 1951, Physical Review, 82, 625
Chandrasekhar, S. 1931a, MNRAS, 91, 456
Chandrasekhar, S. 1931b, ApJ, 74, 81
Chandrasekhar, S. 1935, MNRAS, 95, 207
Chandrasekhar, S. 1939, An Introduction to the Study of Stellar Structure (Chicago, Ill., The University of Chicago Press)
Chandrasekhar, S., & Tooper, R. F. 1964, ApJ, 139, 1396
Dahn, C. C., Bergeron, P., Liebert, J., et al. 2004, ApJ, 605, 400
Das, U., & Mukhopadhyay, B. 2012, Phys. Rev. D, 86, 042001
Fowler, R. H. 1926, MNRAS, 87, 114

Gao, Z. F., Wang, N., Peng, Q. H., Li, X. D., & Du, Y. J. 2013, Modern Physics Letters A, 28, 1350138

Gao, Z. F., Wang, N., Yuan, J. P., Jiang, L., & Song, D. L. 2011, Ap&SS, 332, 129

Hicken, M., Garnavich, P. M., Prieto, J. L., et al. 2007, ApJ, 669, L17

Howell, D. A., Sullivan, M., Nugent, P. E., et al. 2006, Nature, 443, 308

Kepler, S. O., Kleinman, S. J., Nitta, A., et al. 2007, MNRAS, 375, 1315

Landau, L. D., & Lifshitz, E. M. 1980, Statistical Physics Pt.1, (Oxford: Pergamon Press, 3rd ed.)

Li, X. H., Gao, Z. F., Li, X. D., et al. 2016, International Journal of Modern Physics D, 25, 1650002

Malheiro, M., Rueda, J. A., & Ruffini, R. 2012, PASJ, 64, 56

Oppenheimer, J. R., & Volkoff, G. M. 1939, Physical Review, 55, 374

Press, W. H. 1988, Numerical Recipes in C (Cambridge: Cambridge Univ. Press)

Rotondo, M., Rueda, J. A., Ruffini, R., & Xue, S.-S. 2011, Phys. Rev. D, 84, 084007

Salpeter, E. E. 1961, ApJ, 134, 669

Scalzo, R. A., Aldering, G., Antilogus, P., et al. 2010, ApJ, 713, 1073

Shapiro, S. L., & Teukolsky, S. A. 1983, Black Holes, White Dwarfs, and Neutron Stars: The Physics of Compact Objects (New York: Wiley-Interscience)

Silverman, J. M., Ganeshalingam, M., Li, W., et al. 2011, MNRAS, 410, 585

Singh, R. P. 1957, ApJ, 126, 213

Stoner, E. C. 1929, The London, Edinburgh, and Dublin Philosophical Magazine and Journal of Science, 7, 63

Tolman, R. C. 1939, Physical Review, 55, 364

Wapstra, A. H. & Bos, K. 1977, Atomic Data and Nuclear Data Tables, 19, 177 (*https://doi.org/10.1016/0092-640X(77)90020-1*)

Zhu, C., Gao, Z. F., Li, X. D., et al. 2016, Modern Physics Letters A, 31, 1650070